Advanced Steel Construction – Vol. 18 No. 4 (2022) 793–803
DOI:10.18057/IJASC.2022.18.4.7

FATIGUE TESTS OF COMPOSITE DECKS WITH MCL CONNECTORS

Ping-Ming Huang, Xiao-Long Li *, Kui-Hua Mei and Yue Zhao

School of Highway, Chang'an University, Xi'an, China
** (Corresponding author: E-mail: 1047829409@qq.com)*

ABSTRACT

Full-scale fatigue tests were performed on three composite decks with the MCL (modified clothoid) connectors to investigate their fatigue performance. Fatigue life and failure mode of the composite bridge decks were explored by measuring the specimens with three different stress amplitudes. The deflection, strain, carrying capacity, and stiffness degradation of the composite decks were measured and analyzed in the test. In addition, parameter analysis was performed using finite-element method in this study. Results showed that the mechanical performance of the composite decks accorded with the plane-section assumption under constant amplitude load, and the fatigue failure mode of the composite decks was the local fracture of the bottom steel plate. The stiffness degradation law and S-N curve were obtained in this study. Moreover, the concrete slab depth had a remarkable effect on the fatigue performance of the composite decks.

ARTICLE HISTORY

Received: 22 February 2022
Revised: 6 June 2022
Accepted: 8 June 2022

KEYWORDS

Corrugated steel-concrete composite decks;
MCL connectors;
Fatigue test;
Constant amplitude load;
Cracks

1. Introduction

Steel-concrete composite structures are generally used in buildings, bridges, underground structures, and other construction fields due to their excellent bearing capacity, high stiffness, convenient construction, and short construction period [1-3].

Bridge decks often suffer from severe damage under the long-term action because of directly bearing vehicular loads. In this situation, the composite structures composed of corrugated steel, reinforced concrete slab, and steel connectors have been proposed to overcome the limitation of the shear performance of the bridge decks under the heavy vehicular loads. Corrugated steel-concrete composite decks have the advantage of small weight and large bearing capacity over reinforced concrete beams. Compared with orthotropic steel decks, the corrugated steel-concrete composite slab structures can eliminate vulnerable details at the welded junctions of the orthotropic steel bridge decks and reduce the impact of stress concentration and problems caused by the fatigue load [4,5].

Nowadays the static behavior of the composite deck has been extensively investigated by scholars [6-10]. To study the static properties of the composite decks with bolted connectors, Patel analyzed the shear behavior of the connectors with ABAQUS [11]. Mirza performed the numerical simulation and experimental test to investigate the strength of headed studs in the composite decks [12]. Bahaz investigated the influence of the effective width on the composite beams through parameter analysis and proposed design formulas for the composite beams [13]. Wang analyzed the stress at the weld joints of the steel bridge according to the LEFM theory [14]. Chen developed a vehicle model to simulate the bridges in service [15].

Due to their aesthetics and practicability [16], the profiled steel plates are primarily used in the composite deck systems [17]. With the rapid development of the transportation, vehicular loads may cause fatigue damage in the composite beams [18]. Hence, it is necessary to study the fatigue performance of the corrugated steel-concrete composite decks. However, the study on the dynamic behavior of the composite decks is limited [19-22]. The bearing capacity and stiffness of the composite decks will degrade to a certain extent due to the effect of fatigue loads [23]. Fatigue damage causes failures of the composite decks. Therefore, studying the fatigue behavior of the composite decks is essential.

This study investigated a novel type of composite structure [24]. It consisted of concrete deck, corrugated steel plate, MCL (modified clothoid) connectors, and reinforcements, as shown in Fig. 1. Compared with the headed studs, the MCL connectors exhibit the advantage of higher load-bearing capacity [25]. In this study, three specimens were performed under the fatigue load to explore the fatigue characteristics. The fatigue life and failure mode of the composite bridge decks were evaluated under different stress amplitudes. Factors influencing the fatigue behavior of the composite decks were analyzed by the finite-element method (FEM). The significance of this research is helpful for the anti-fatigue design of the composite decks.

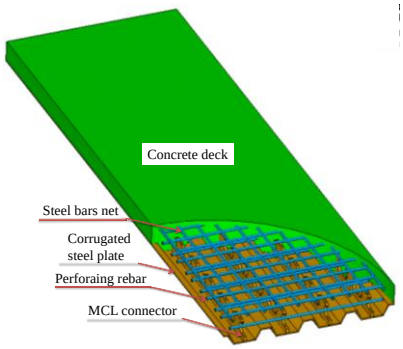

Fig. 1 Corrugated steel-concrete composite decks

2. Testing program

2.1. Dimensions of the composite deck

Three 1:1 full-scale corrugated steel-concrete composite bridge decks (1000 mm × 180 mm × 3100 mm) with MCL connectors were fabricated and tested to examine their fatigue performance. Table 1 presents the dimensions of the composite decks and Fig. 2 shows the shape of the cross-section. The details of the cross-section are listed in Table 2. The MCL connectors (3000 mm × 14 mm × 110 mm) are illustrated in Fig. 3. Steel components made of Q345 were fabricated in the factory. The MCL connectors were welded to the steel plate and the concrete deck made of C50 was cast in place after erection of the formwork. Fig. 4 shows the fabrication of the composite decks.

2.2. Material properties

Standard cube blocks were prepared for each composite deck specimen. They were cured under the same circumstance as the specimens for 28 days. The cubes were tested to obtain the average compressive strength before the fatigue test was performed. The yield and ultimate strength of the steel structures were evaluated in the tensile test. Table 3 presents the details of the material properties.

Table 1
Parameters of the composite bridge decks (unit: mm)

No.	*L*	*W*	*H*	*T*	MCL connector spacing		Longitudinal	Transverse
					Longitudinal spacing	Transverse spacing	Bars	Bars
FT-1	3100	1000	180	6	200	250	A16 × 10@10	A16×64@10
FT-2	3100	1000	180	6	200	250	A16 × 10@10	A16×64@10
FT-3	3100	1000	180	6	200	250	A16 × 10@10	A16×64@10

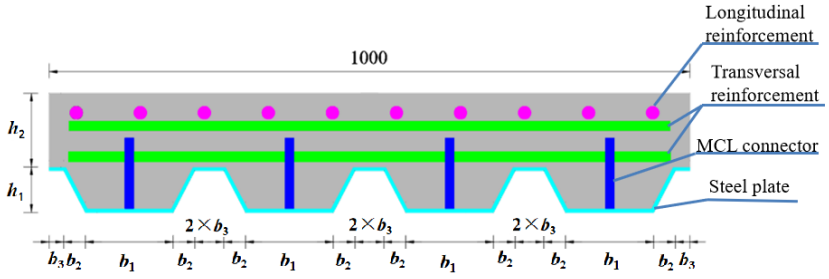

Fig. 2 Cross section (unit: mm)

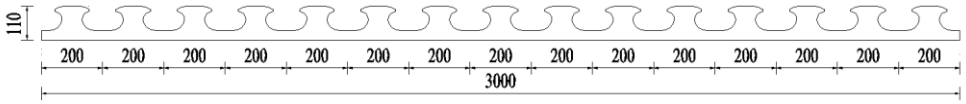

Fig. 3 MCL Connectors (unit: mm)

Table 2
Cross section size of the decks (unit: mm)

Specimen No.	b_1	b_2	b_3	h_1	h_2
FT-1	130	30	30	65	115
FT-2	130	30	30	65	115
FT-3	130	30	30	65	115

(a) Fabrication of the steel structure (b) Erection of the formwork

Fig. 4 Fabrication of the composite deck

Table 3
Material properties of the composite deck specimens (unit: MPa).

Specimen No.	Corrugated steel plate		MCL connectors		f_{cu} (MPa)
	f_y (MPa)	f_u (MPa)	f_y (MPa)	f_u (MPa)	
FT-1	415.6	568.8	438.6	584.3	62.8
FT-2	416.5	569.2	438.6	584.3	61.5
FT-3	414.9	569.5	438.6	584.3	59.4

Note: f_{cu} = average compressive strength of cubic concrete.

Table 4
Fatigue test variables for composite decks.

Specimen No.	Ultimate bearing capacity P_u	Fatigue Load (kN)		Fatigue load range	Cycle times	Failure mode
	(kN)	Upper Limit	Lower Limit	(kN)	($\times 10^4$)	
FT-1	750	450	90	360	25.7	Fracture of steel plate
FT-2	750	360	90	270	83.1	Fracture of steel plate
FT-3	750	260	90	170	242.0	Fracture of steel plate

2.3. Fatigue test program

2.3.1. Loading scheme

Three specimens were tested under the constant amplitude load, and the 500 kN MTS was used in the fatigue test. Fig. 5 depicts the set-up of the tests. The corrugated steel-concrete composite deck was simply supported, with one end hinged and the other end rolling supported. The fatigue loading frequency was 3 Hz. Details of the fatigue loading scheme are displayed in Table 4.

Firstly, the pre-static test was carried out to determine whether the instruments could work. The pre-static load was 10% to 15% of the maximum fatigue load [26]. The MTS system was halted during the fatigue test, and the static loading would be performed to analyze the residual deflection and stiffness degradation when the number of load cycles approached 1×10^4, 3×10^4, 5×10^4, 10×10^4, 20×10^4, 50×10^4, 150×10^4, and 200×10^4, respectively.

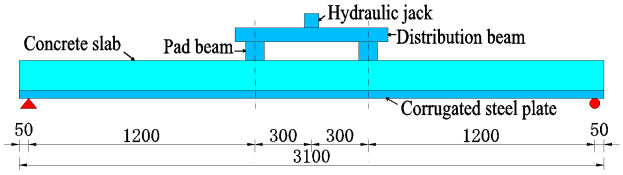

(a) Fatigue loading diagram (unit: mm)

(b) Fatigue loading arrangement

Fig. 5 Fatigue test set-up

2.3.2. Measurement scheme

Ten displacement transducers labeled D1 to D12 were set up to measure the deflection and displacement of the corrugated steel-concrete composite deck. D3 and D8 were used to measure the displacement at the mid-span of the composite deck. D11 and D12 were arranged at the ends of the composite deck to obtain the relative slippage at the interface between the steel plate and the concrete deck.

Fig. 6(a) shows the layout of the displacement transducers. Strain gauges labeled C1 to C4 were used to investigate the concrete strain, and C5 to C15 were used to get the strain of the steel component, as shown in Fig. 6(b).

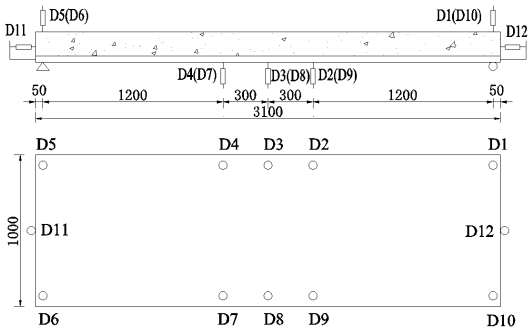

(a) Placement of displacement transducers

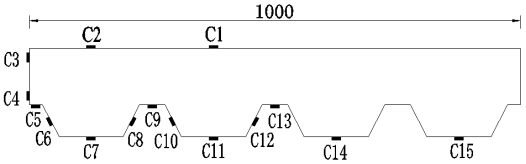

(b) Arrangement of strain gauges

Fig. 6 Layout of the instruments (unit: mm)

3. Results and discussion

3.1. Fatigue failure mode

The fatigue life of specimen FT-1 was 25.7×10^4. For specimen FT-2, it was 83.1×10^4, and 242×10^4 for specimen FT-3. Moreover, their failure mode was the fracture of the steel plate. No cracks were observed at the bottom of the steel plate. One fine crack was discovered at the pure bending section of the composite decks when the cycle number reached a specific value. Fig. 7(a) shows the crack found at the steel plate of specimen FT-3 when the cycle number reached 2.04 million. The fatigue crack extended horizontally to both sides of the steel plate with the increase of the cycle number till the corrugated steel plate failed. Fig. 7(b) shows the crack when the cycle number approached 2.4 million.

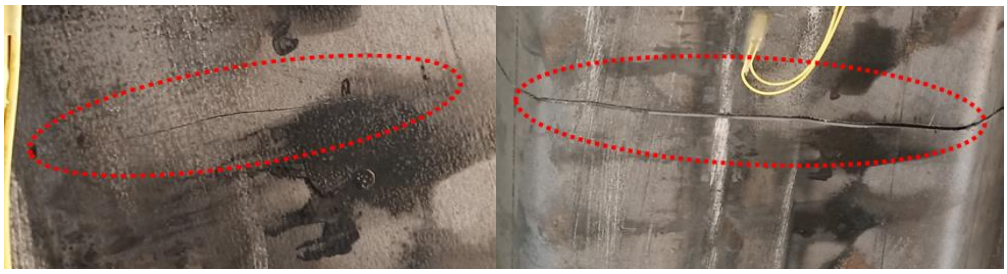

(a) Crack initiation

(b) Development of the fatigue crack

Fig. 7 Fatigue crack

(a) Fatigue failure of FT-1 (b) Cracks at the bottom of FT-1

(c) Fatigue failure of FT-2 (d) Cracks at the bottom of FT-2

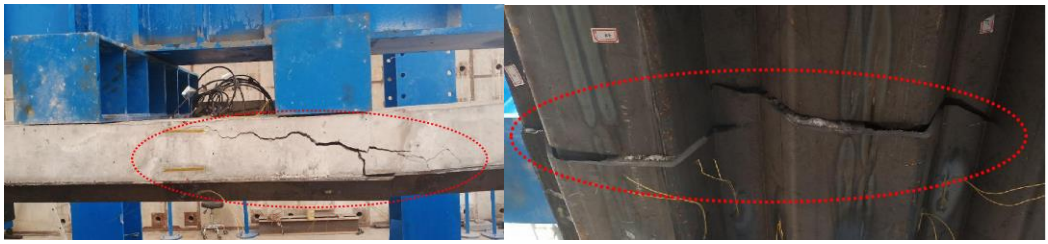

(e) Fatigue failure of FT-3 (f) Cracks at the bottom of FT-3

Fig. 8 Fatigue failure

Fig. 8 illustrates the fatigue failure of the composite decks. The fatigue cracks commonly occurred at the pure bending section of the composite decks, as shown in Fig. 9, which could be attributed to the maximum tensile stress generated there. One Y-shaped crack was observed in the concrete slab. Notably, the cracks were mainly found at the pure bending section of the steel plate. None of them penetrated through the whole steel plate. It could be inferred that the composite deck still had some bearing capacity after fatigue failure. Furthermore, the MCL connectors welded to the steel plate were also broken after the fracture of the steel plate. For specimen FT-3, the failure mode of the concrete deck was different from that of the other two specimens, which could be ascribed to the crack locations. When the cracks did not occur at the pure bending section of the composite decks, the fracture of specimen FT-3 seemed to be diagonal-tension failure, as shown in Figs. 8(e) and (f).

For specimen FT-1, only two cracks penetrated through the lower flange of the steel plate, while for specimen FT-2 and specimen FT-3, three cracks did, as shown in Fig. 9. The reason was that the load amplitude was relatively higher so that specimen FT-1 failed to bear the fatigue load before the crack continued to propagate.

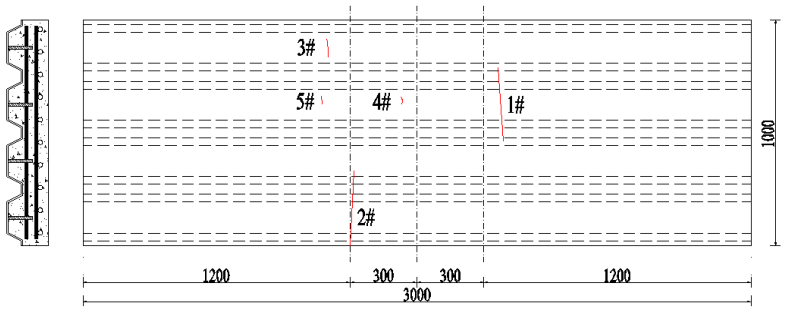

(a) FT-1

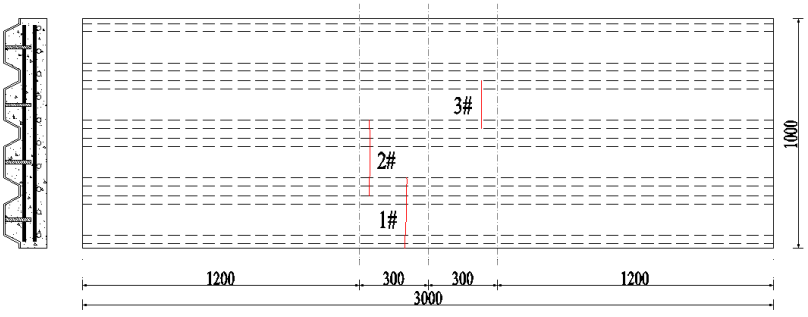

(b) FT-2

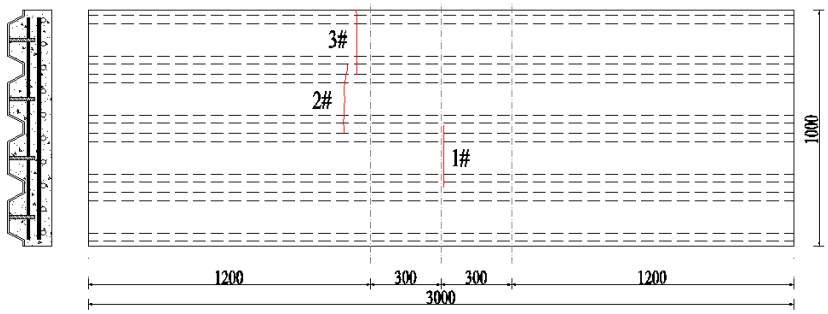

(c) FT-3

Fig. 9 Fatigue cracks of the corrugated steel-concrete composite decks

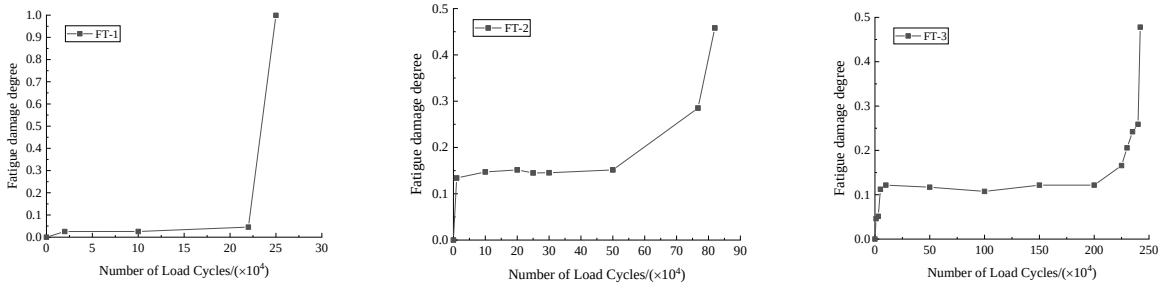

(a) FT-1 (b) FT-2 (c) FT-3

Fig. 10 Fatigue damage degree

3.2. Fatigue damage analysis

To investigate the development of fatigue damage of the composite decks, the fatigue damage degree D_n is adopted in the following equation [27]:

$$D_n=1-B_n/B_0 \quad (1)$$

where B_n is the stiffness of the composite decks at the nth fatigue loading cycle, B_0 is the initial stiffness of the composite decks.

Fig. 10 depicts the relationship of D_n versus n. The development of the fatigue damage could be divided into three stages. The fatigue damage increased sharply in the first stage, and some cracks initiated in the concrete deck. In the second stage, the fatigue damage tended to be stable. In the third stage, cracks initiated in the steel plate and propagated, and finally the composite deck failed to bear the fatigue load due to the crack propagation. During this stage, the fatigue damage increased rapidly.

By comparing the fatigue damage degree of the three composite decks, it could be found that the D_n of specimen FT-1 was lower than that of specimens FT-2 and FT-3 in the first two stages. However, in the third stage, the D_n of specimen FT-1 was twice as large as that of specimens FT-2 and FT-3. This might be that the fatigue load amplitude of specimen FT-1 was larger than that of specimens FT-2 and FT-3, which meant that once specimen FT-1 had fatigue damage, it would be destroyed in a short time under the fatigue load.

Fig. 11 shows the stiffness degradation and the curve fitting of FT-2 and FT-3. The relationship of stiffness degradation and the cycle number of FT-2 and FT-3 can be expressed by Equations (2) and (3), respectively. The fitting precision of Equations (2) and (3) are 0.9979 and 0.9737, respectively.

$$\frac{B_n}{B_0}=1-0.55107\times\left\{0.24282\times\left(\frac{n}{N}\right)^{2.93956E-10}+0.58875\times\left[1-\left(1-\frac{n}{N}\right)^{0.21683}\right]\right\} \quad (2)$$

$$\frac{B_n}{B_0}=1-0.47898\times\left\{0.15554\times\left(\frac{n}{N}\right)^{0.02458}+0.84446\times\left[1-\left(1-\frac{n}{N}\right)^{0.12344}\right]\right\} \quad (3)$$

where and N is the fatigue life.

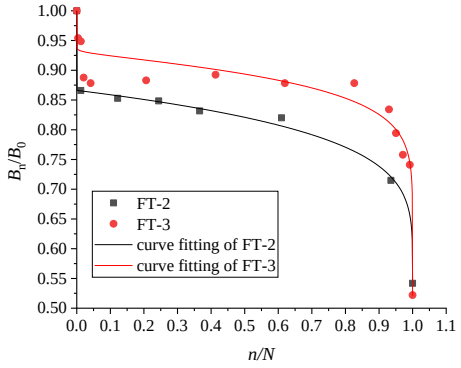

Fig. 11 Stiffness degradation

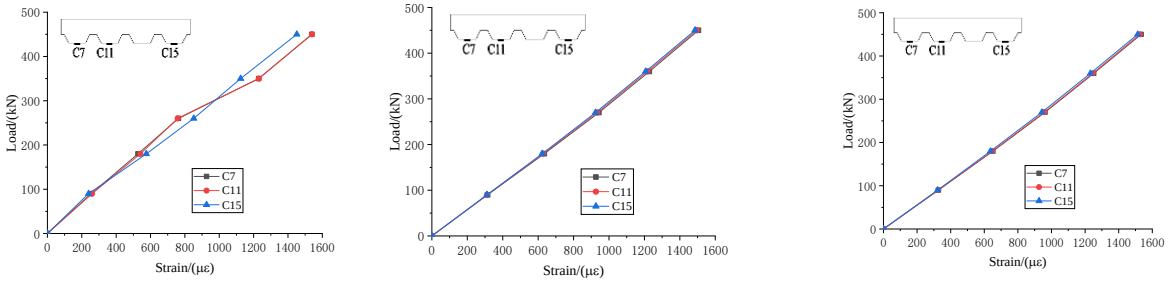

(a) 0 (b) 10000 (c) 220000

Fig. 12 Strain variations of FT-1 specimen under different loading cycles

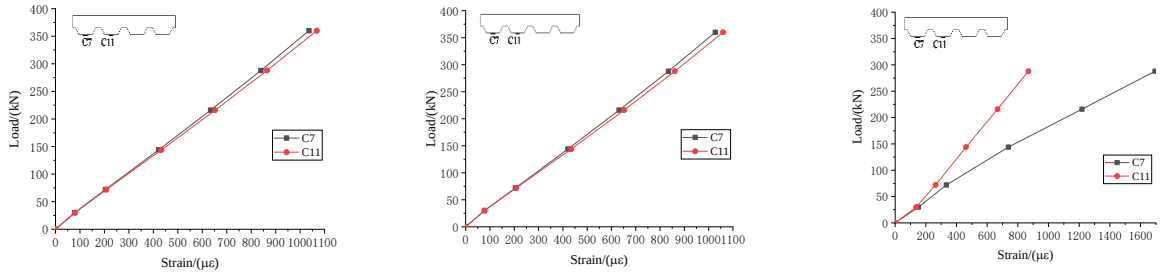

(a) 0 (b) 500,000 (c) 831,000

Fig. 13 Strain variations of FT-2 specimen under different loading cycles

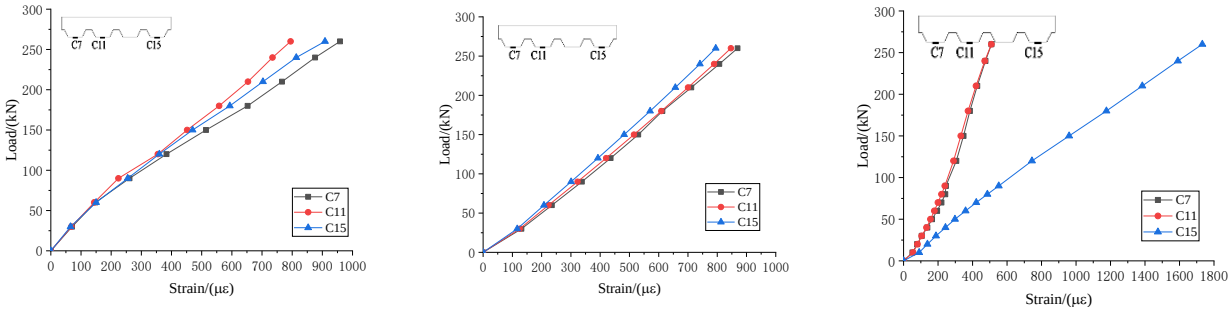

(a) 0 (b) 2 million (c) 2.42 million

Fig. 14 Strain variations of FT-3 specimen under different loading cycles

3.3. Strain analysis

Figs. 12, 13, and 14 show the strain variations of the steel plate under different load cycles, respectively. The strain variations of the steel plate were identical and linear under lower fatigue load, as shown in Figs. 12(a), 13(a), and 14(a). However, for FT-2, strains at C3 were lower than strains at C11 under identical load. This might be the reason that the bottom flanges to which the strain gauges with lower strains were attached fractured under fatigue load, while the undamaged bottom flanges at other parts of the composite deck continued to bear the fatigue load, as shown in Figs. 13(c) and 14(c).

Figs. 15, 16, and 17 present the strain variations at the mid-span of the specimens under different number of load cycles, respectively. The strain variations along the height direction of the composite deck were basically linear during the fatigue test. It was indicated that the composite bridge decks satisfied the plane-section hypothesis when the static load value was relatively lower.

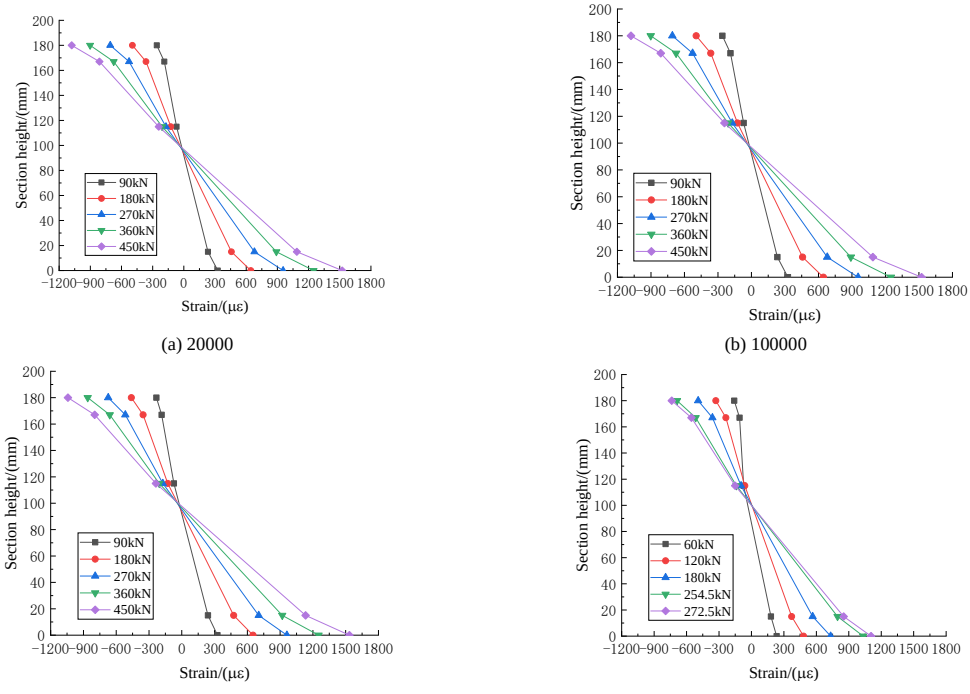

(a) 20000 (b) 100000

(c) 220000 (d) 257000

Fig. 15 Strain variations of specimen FT-1

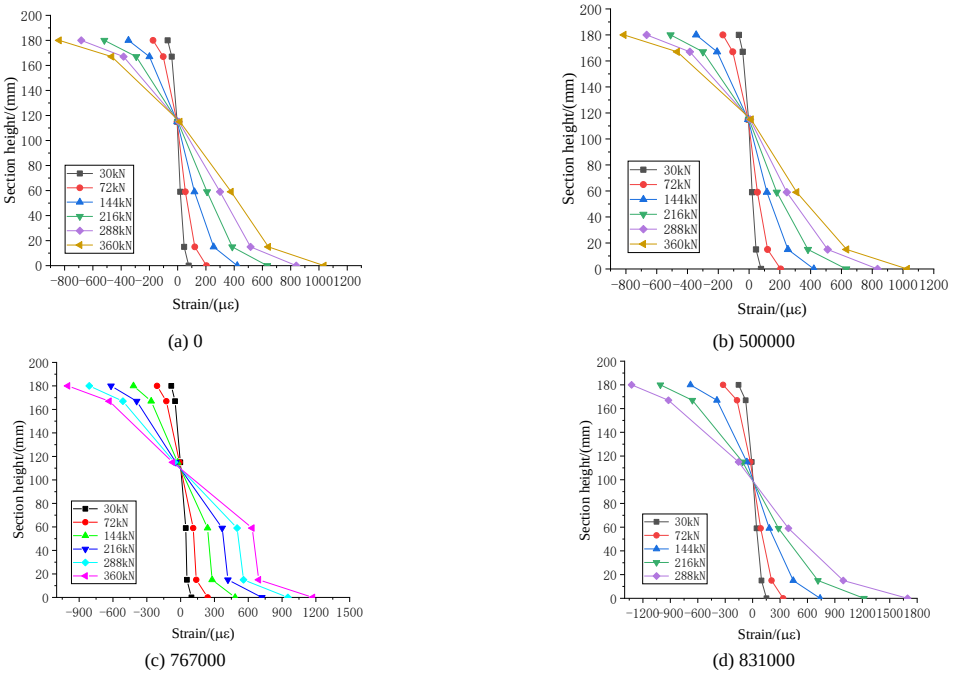

(a) 0 (b) 500000

(c) 767000 (d) 831000

Fig. 16 Strain variations of specimen FT-2

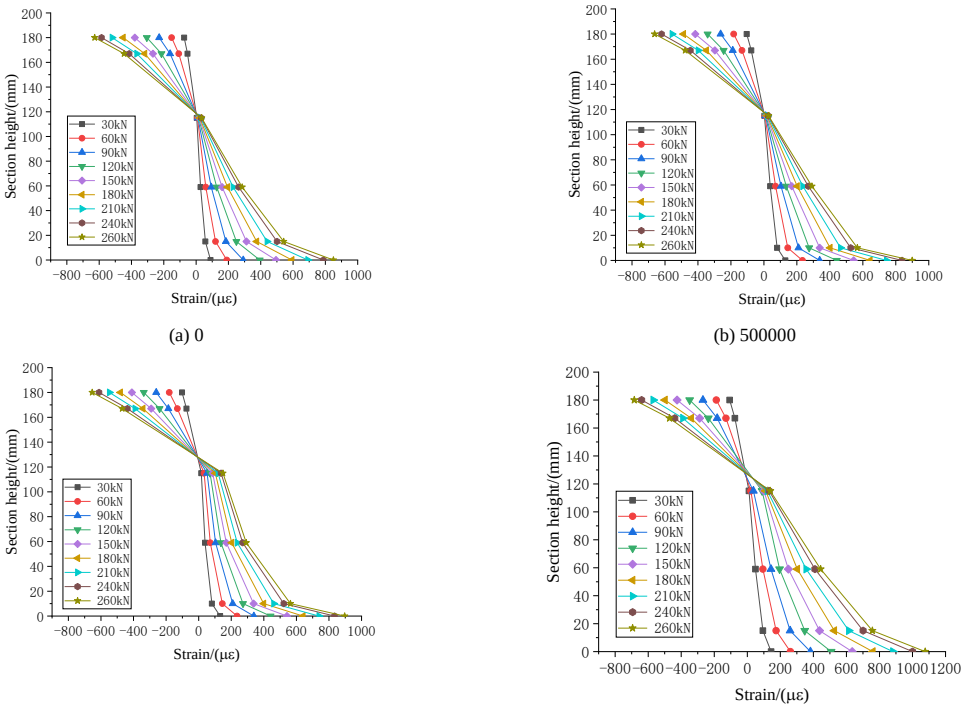

(a) 0 (b) 500000

(c) 1500000 (d) 2400000

Fig. 17 Strain variations of specimen FT-3

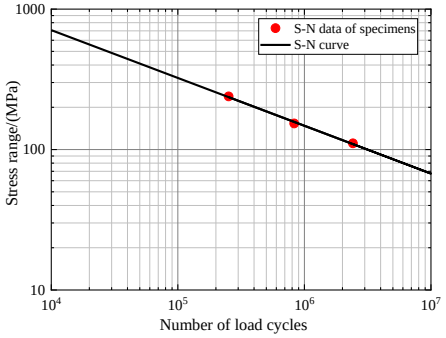

Fig. 18 S-N curve fitting of specimens

3.4. Statistical evaluation of stress category

The S-N curve of the specimens was obtained by fitting the results of the fatigue test, as shown in Fig. 18. The fatigue life of specimens can be expressed as follows:

$$Log_{10}\Delta\sigma + 0.3405 Log_{10}N = 4.21237 \quad (4)$$

where $\Delta\sigma$ represents the tensile stress amplitude; N represents the fatigue life.

3.5. Residual bearing capacity

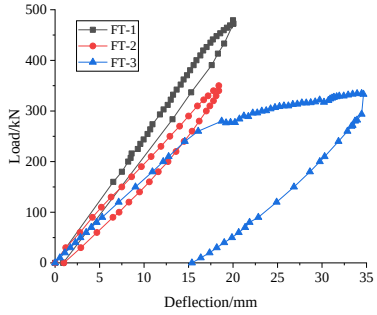

Fig. 19 Residual bearing capacity of the composite decks

The static test was performed to obtain the residual bearing capacity of the specimens when they failed to bear the fatigue load. Fig. 19 depicts the displacement of the composite decks under the static load. The residual carrying capacity of specimen FT-1 was 479.2 kN (0.639 P_u). For FT-2, the residual carrying capacity was 330 kN (0.440 P_u). For FT-3, the residual carrying capacity was 334.5 kN (0.446 P_u). The investigation on the residual bearing capacity of the composite decks would be helpful for the reinforcement and maintenance.

4. Parameter analysis

4.1. Fatigue load model

The fatigue vehicle model should be adopted to get the stress history of the fatigue concern points. There are three types of anti-fatigue design in JTG D64 [28]. The first type adopts equivalent lane load, called the fatigue load calculation model I. The second type adopts the double-vehicle model, called the fatigue load calculation model II. The model details are shown in Fig. 20. The third type adopts a singular-vehicle model, called the fatigue load calculation model III, Fig. 21 shows the details of the fatigue vehicle model. The model III can be used to calculate the bridge deck components. Two loading schemes, the central loading and the eccentric loading, were implemented to obtain the stress at different fatigue concern points. Fig. 22 shows the schematic diagram of the fatigue load layout.

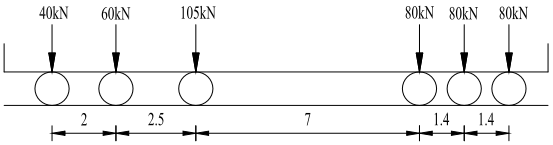

Fig. 20 Model Ⅱ (unit: m)

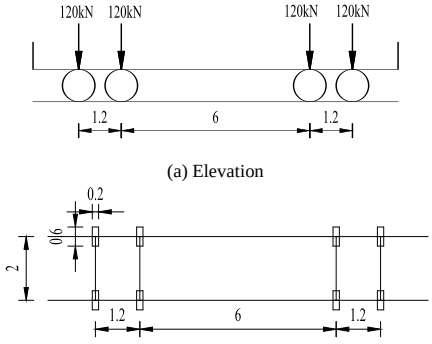

Fig. 21 Model Ⅲ (unit: m)

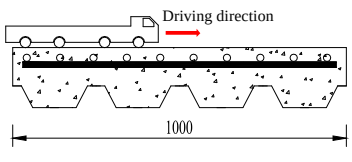

(a) Driving direction

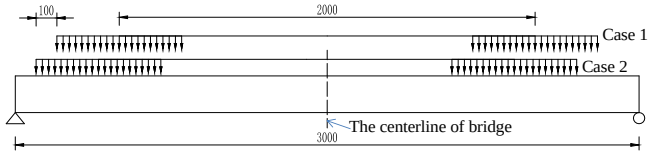

(b) Loading cases

Fig. 22 Schematic diagram of fatigue load layout (unit: mm)

4.2. Numerical analysis model

The numerical analysis model was established using the finite-element method to investigate the influence of the concrete slab depth, the steel plate thickness, and the concrete strength on the fatigue performance of the composite decks. The solid element was applied to the simulation of the composite decks, as depicted in Fig. 23. The relative slippage between the concrete deck and steel plate was ignored. The elastic modulus and Poisson ratio of steel are 2.06×10^5 MPa and 0.3, respectively. For the concrete deck, they are 3.45×10^4 MPa and 0.2, respectively.

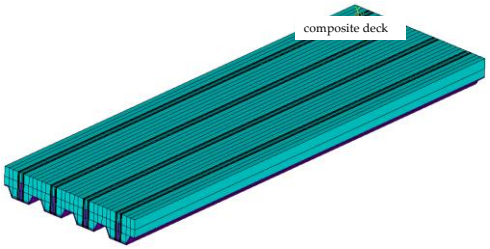

(a) Geometric model

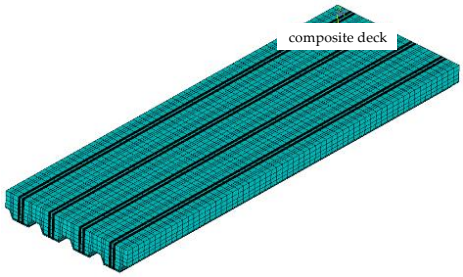

(b) Mesh model

Fig. 23 FEM model

Due to the fact that the steel plate fracture occurred near the mid-span of the composite decks during the test. Two points numbered 1 and 2 were selected to investigate the stress history, and their locations were at the mid-span of the steel plate. Fig. 24 shows the details of the points' locations.

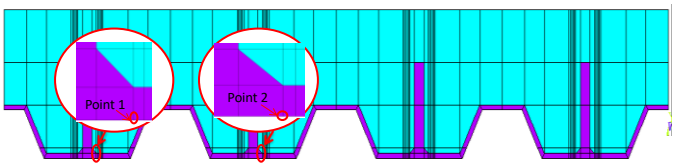

Fig. 24 Fatigue points

The analysis of stress history was beneficial for understanding the fatigue behavior of the composite decks. The model III was employed to investigate the stress variation of the fatigue concern points under different conditions, Table 5 lists the tensile stress at different points.

Table 5
Fatigue test variables for composite decks (unit: MPa)

No.	JTG D64	
	Case 1	Case 2
1	23.62	23.42
2	23.40	23.42

By comparing the stress variations at the two fatigue concern points with

each other, the maximum tensile stresses at Points 1 and 2 were approximately similar, as shown in Fig. 25. Vehicles passing through the composite decks would cause the different load amplitudes. Different load amplitudes can be represented by the equivalent stress amplitude [29] based on the Miner standard to estimate the fatigue characteristics of the composite decks in a simple way [30]. The equivalent stress amplitude can be calculated by Eq. (5).

$$\Delta\sigma_0 = \left[\frac{\sum n_i (\Delta\sigma_i)^m}{N_0}\right]^{\frac{1}{m}} \tag{5}$$

where n_i is the cycle number of stress range $\Delta\sigma_i$; $\Delta\sigma_i$ is the stress amplitude corresponding to the ith cycle loading; $\Delta\sigma_0$ is the equivalent stress range; N_0 is the cyclic number concerning $\Delta\sigma_0$; m is a constant.

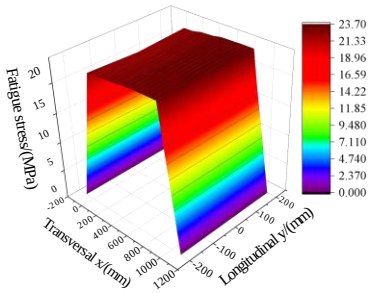

(a) Point 1

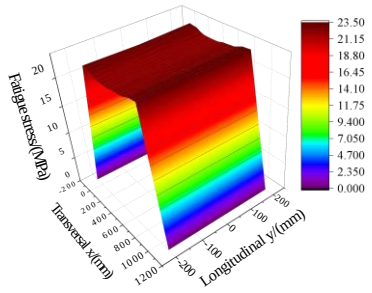

(b) Point 2

Fig. 25 Tensile stress at different positions

The loading method Case 1 was adopted to explore the $\Delta\sigma_0$ of the concern points. The stresses at each point under different load cases were similar, as shown in Fig. 26. Table 6 presents the tensile stress amplitude and the corresponding equivalent stress amplitude. Calculated by Eq. (4), the fatigue life of the composite deck at Point 1 under Case 1 was 119 million. The results showed that the specimens' fatigue resistance was excellent.

To analyze the factors affecting the fatigue performance of the composite decks, three parameters, including the concrete strength, the concrete slab depth and the steel plate thickness, were selected in this study. Fatigue concern Point 1 was selected as an example for the parameter analysis, and Case 1 was selected as the normative fatigue vehicle loading layout.

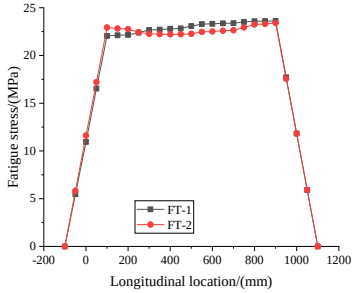

(a) Case 1

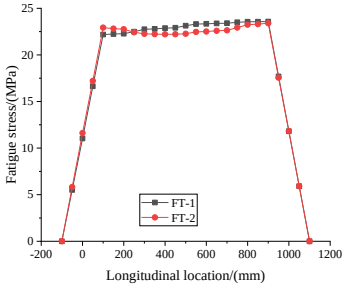

(b) Case 2

Fig. 26 Tensile stress at different positions

Table 6
Tensile stress amplitude at different fatigue concern points

Concern points	Tensile stress amplitude (MPa)	Number of cycles	Equivalent stress amplitude (MPa)
1	23.62	1	23.62
2	23.40	1	18.57
	1.19	1	

4.3. Strength variation of concrete slab

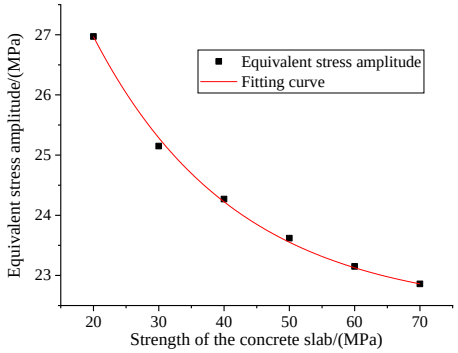

(a)

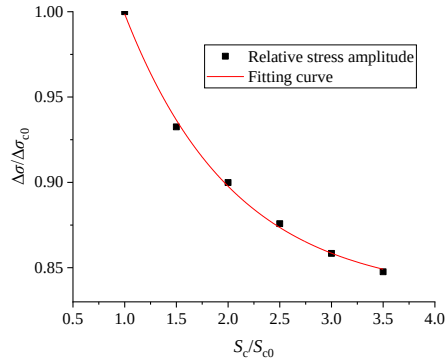

(b)

Fig. 27 Relation of the concrete strength vs. the equivalent stress amplitude

Six concrete strength grades were adopted in the FEM analysis to study the relation of the concrete strength versus the equivalent stress amplitude. The equivalent stress amplitude $\Delta\sigma$ decreased with the increase of the concrete strength S_c. When $\Delta\sigma/\Delta\sigma_{c0}$ increased from 1 to 3.5 (by 250%), S_c/S_{c0} decreased from 1 to 0.85 (by 15%), as shown in Fig. 27. It could be concluded that the influence of the concrete strength above 50 MPa was relatively lower on the fatigue characteristics of the composite decks. The formulas of S_c versus $\Delta\sigma$ at Point 1 can be described as follows:

$$\frac{\Delta\sigma}{\Delta\sigma_{c0}} = 0.4252e^{\left(-\frac{S_c}{S_{c0}}\right)} \tag{6}$$

where S_c is the concrete strength; $\Delta\sigma_{c0}$ is the equivalent stress amplitude corresponding to S_{c0}; S_{c0} = 20 MPa.

4.4. Depth of concrete slab

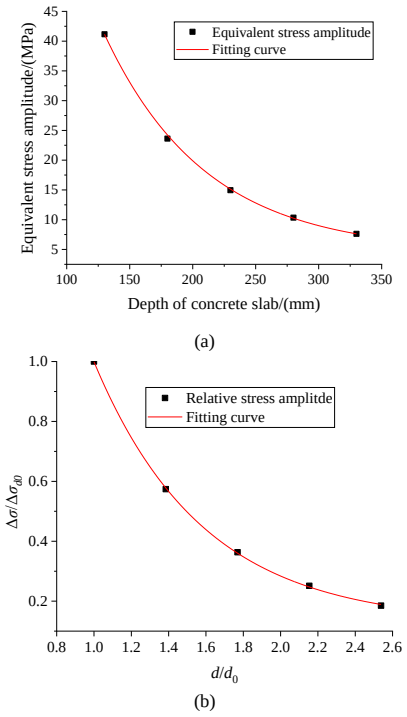

Fig. 28 Relation of the concrete deck depth vs. the equivalent stress amplitude

The concrete slab depth (abbreviated as d) was adopted as 130 mm, 180 mm, 230 mm, 280 mm, and 330 mm in the FEM analysis. The equivalent stress amplitude decreased significantly with the increase of d, as shown in Fig. 28(a). When d/d_0 increased from 1.0 to 2.5 (by 150%), the $\Delta\sigma/\Delta\sigma_{d0}$ decreased from 1 to 0.2 (by 80%). The relationship between $\Delta\sigma$ and d obtained from Fig. 28(b) can be expressed as follows:

$$\frac{\Delta\sigma}{\Delta\sigma_{d0}} = 4.83e^{\left(-\frac{d}{0.58d_0}\right)} \tag{7}$$

where d is the concrete deck depth and the value of d_0 is 130 mm $\Delta\sigma_{d0}$ is the equivalent stress amplitude corresponding to d_0.

4.5. Thickness of steel plate

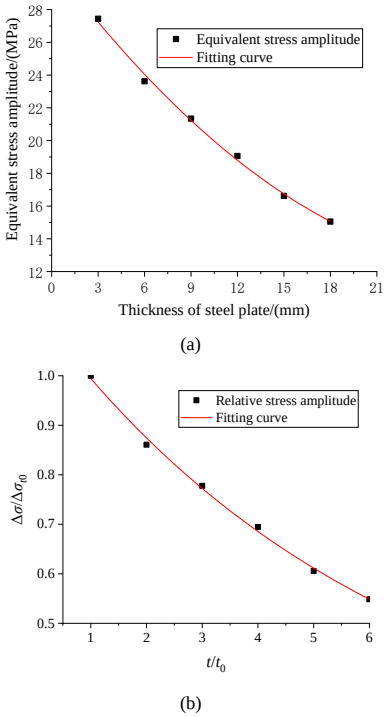

Fig. 29 Relation of steel plate thickness vs. the equivalent stress amplitude

The thickness of the steel plate (abbreviated as t) was set at 3 mm, 6 mm, 9 mm, and 12 mm. Fig. 29(a) depicts the variation of $\Delta\sigma_0$. When t/t_0 increased from 1 to 6 (by 500%), $\Delta\sigma/\Delta\sigma_{t0}$ decreased from 1 to 0.54 (by 46%). For the composite decks, the influence of steel plate thickness was evident. According to Fig. 29(b), the relationship between t and $\Delta\sigma_0$ can be obtained by the following:

$$\frac{\Delta\sigma}{\Delta\sigma_{t0}} = 29.04 - \frac{0.81t}{t_0} \tag{8}$$

where t is the thickness of steel plate and t_0 is 3 mm; $\Delta\sigma_{t0}$ is the equivalent stress amplitude corresponding to t_0.

The concrete slab depth had a remarkable influence on the fatigue performance of the composite decks. And the influence of the concrete slab strength on the fatigue performance of the composite decks was little.

5. Conclusions

Three full-scale specimens were examined via fatigue tests and the fatigue performance of the composite bridge decks was analyzed using FEM.

The fatigue failure of the composite decks typically occurred near the mid-span of the composite decks. Cracks initiated in the pure bending section of the composite decks and propagated transversely with the increase of cycle number, and finally led to the failure of the composite decks.

The stiffness degradation law and the S-N curve of the composite decks had been obtained in this paper. It was found that the influence of the concrete slab depth on the fatigue performance of the composite decks was remarkable.

References

[1] Nie J., Wang Y., “Research status on fatigue behavior of steel-concrete composite beams”, Eng. Mech., 29(6), 1-11, 2012.
[2] Zhang Q., Yuan D., Wang B., et al, “Fatigue performance of innovative both-side welded rib-to-deck joints”, China J Highs Transp, 33(5), 79-91, 2020.
[3] Pardeshi R. T., Patil Y. D., “Review of various shear connectors composite structures”, Adv. Steel Constr., 17(4), 394-402, 2021.
[4] Zhang Q., Bu Y., Li Q., “Review on fatigue problems of orthotropic steel bridge deck”, China J Highw Transp, 2017; 30(3): 14-30.
[5] Kim H. Y., Jeong Y. J., “Experimental investigation on behavior of steel–concrete composite bridge decks with perfobond ribs”, J Constr Steel Res, 2006 ,62(5): 463-471.
[6] Kim H. Y., Jeong Y. J., “Experimental investigation on behavior of steel-concrete composite bridge decks with perfobond ribs”, J Constr Steel Res, 2006, 62(5): 463-471.
[7] Kim H. Y., Jeong Y. J., “Ultimate strength of a steel-concrete composite bridge deck slab with profiled sheeting”, Eng Struct, 2010, 32(2): 534-546.
[8] Kim H. Y., Jeong Y. J., “Steel-concrete composite bridge deck slab with profiled sheeting”, J Constr Steel Res, 2009, 65(8-9): 1751-1762.
[9] Jeong Y. J., Kim H. Y., Koo H. B., “Longitudinal shear resistance of steel-concrete composite slabs with perfobond shear connectors”, J Constr Steel Res, 2009, 65(1), 81-88.
[10] Jeong Y. J., “Simplified model to predict partial-interactive structural performance of steel-concrete composite slabs”, Journal of Constructional Steel Research, 2008, 64(2), 238-246.
[11] Patel V. I., Uy B., Pathirana S. W., et al., “Finite element analysis of demountable steel-concrete composite beams under static loading”, Adv. Steel Constr., 14(3), 392-411, 2018.
[12] Mirza O., Uy B., “Effects of strain regimes on the behaviour of headed stud shear connectors for composite steel-concrete beams”, Adv. Steel Constr., 6(1), 635-661, 2010.
[13] Bahaz A., Amara S., Jaspart J. P., et al., “Numerical analysis and evaluation of effective slab width of composite continuous beams with semi-rigid joint”, Adv. Steel Constr., 17(4), 331-339, 2021.
[14] Wang C. S., Zhai M. S., Duan L., et al., “Fatigue service life evaluation of existing steel and concrete bridges”, Adv. Steel Constr., 11(3), 305-321, 2015.
[15] Chen W. Z., Xu J., Yan B. C., et al. “Fatigue load model for highway bridges in heavily loaded areas of China”, Adv. Steel Constr., 11(3), 322-333, 2015.
[16] Islam S., Abang-Abdullah A. A., Jafar M. S., “An investigation on structural performance of profiled steel to develop self-supporting roofing system”, Adv. Steel Constr., 2(1), 87-108, 2006.
[17] Ayman E., Hani S., Aaron S., “Fatigue tests on steel-concrete composite beams subjected to sagging moments”, J Struct Eng, 2019, 145(5): 04019029.
[18] Liu R., Yang Y., Zhou X., “Experimental study on fatigue performance of composite beam with steel-plate-concrete composite decks”, Constr Build Mater, 2018, 188: 833-849.
[19] Ahn J. H., Sim C., Jeong Y. J., et al., “Fatigue behavior and evaluation of the stress category for a steel-concrete composite bridge deck”, J Constr Steel Res 2009, 65(2), 373-385.
[20] Gao Q., Dong Z., Cui K., et al., “Fatigue performance of profiled steel sheeting-concrete bridge decks subjected to vehicular loads”, Eng Struct 2020, 213: 110558.
[21] Schuster R. M., Suleiman R. E., “Composite slabs subjected to repeated point loading”, Eighth International Specialty Conference on Cold-Formed Steel Structures ST. Louis, Missouri, U.S.A., 1986, November, 453-485.
[22] Mouw K. W., “Fatigue testing of light gage metal forms”, Center for Cold-Formed Steel Structures Library, 1969, January, 1-35.
[23] Yang Y., Nie J., Du M., et al., “Study on fatigue performance of closed profiled steel sheeting-concrete composite slabs”, Civil Eng J, 2008, 41(12), 35-41.
[24] Kong F., Huang P., Han B., Wang X., Liu C., “Experimental study on behavior of corrugated steel-concrete composite bridge decks with MCL shape composite dowels”, Eng Struct,

2021, 227, 111399.
[25] Kopp M., Wolters K., Classen M., et al., “Composite dowels as shear connectors for composite beams-Background to the design concept for static loading”, J Constr Steel Res, 2018, 147, 488-503.
[26] Nie J., “Steel-concrete Composite Beams: Experiment, Theory and Application”, Beijing: Science Press; 2005.
[27] Hu R., Fang Z., Jiang R., Xiang Y., Liu C., “Fatigue prediction model of ultra-high-performance concrete beams prestressed with CFRP tendons”, Adv Struct Eng, 2021, 25, 3, 611-624.
[28] JTG D64-2015. Specification for Design of Highway Steel Bridge. Chinese specification, 2015.
[29] Miner M. A., “Cumulative damage in fatigue”, J. Appl. Mech. 1945, 12, 159-164.
[30] Huang Y., Zhang Q. H., Bao Y., Bu Y., “Fatigue assessment of longitudinal rib-to-crossbeam welded joints in orthotropic steel bridge decks”, J. Constr. Steel Res. 2019, 159, 53-66.